

## Laboratory demonstration of single-camera PPPP wavefront sensing using neural networks

Carlos Gonzalez-Gutierrez, Nazim Ali Bharmal, Jorge Rodriguez-Muro, Alejandro Buendia-Roca, Huizhe Yang, Laurence W. Fitzpatrick, Timothy J. Morris & Francisco Javier de Cos Juez

**To cite this article:** Carlos Gonzalez-Gutierrez, Nazim Ali Bharmal, Jorge Rodriguez-Muro, Alejandro Buendia-Roca, Huizhe Yang, Laurence W. Fitzpatrick, Timothy J. Morris & Francisco Javier de Cos Juez (2024) Laboratory demonstration of single-camera PPPP wavefront sensing using neural networks, International Journal of Optomechatronics, 18:1, 2386985, DOI: [10.1080/15599612.2024.2386985](https://doi.org/10.1080/15599612.2024.2386985)

**To link to this article:** <https://doi.org/10.1080/15599612.2024.2386985>



© 2024 The Author(s). Published with license by Taylor & Francis Group, LLC



Published online: 21 Aug 2024.



Submit your article to this journal [↗](#)



Article views: 140



View related articles [↗](#)



View Crossmark data [↗](#)

# Laboratory demonstration of single-camera PPPP wavefront sensing using neural networks

Carlos Gonzalez-Gutierrez<sup>a,b</sup>, Nazim Ali Bharmal<sup>c</sup>, Jorge Rodriguez-Muro<sup>a</sup>, Alejandro Buendia-Roca<sup>a,d</sup>, Huizhe Yang<sup>e</sup>, Laurence W. Fitzpatrick<sup>c,f</sup>, Timothy J. Morris<sup>c</sup>, and Francisco Javier de Cos Juez<sup>a,d</sup>

<sup>a</sup>Instituto Universitario de Ciencias y Tecnologías Espaciales de Asturias (ICTEA), Oviedo, Spain; <sup>b</sup>Computer Sciences Department, University of Oviedo, Gijón, Spain; <sup>c</sup>Centre for Advanced Instrumentation, Department of Physics, Durham University, Durham, UK; <sup>d</sup>Department of Exploitation and Prospection of Mines, Oviedo, Spain; <sup>e</sup>College of Advanced Interdisciplinary Studies, National University of Defense Technology, Changsha, China; <sup>f</sup>Department of Biomedical Engineering, Institute for Complex Molecular Systems (ICMS), Eindhoven University of Technology, Eindhoven, The Netherlands

## ABSTRACT

Laser guide stars in astronomical adaptive optics systems have the focus anisoplanatism problem, especially for telescopes larger than 4 m in diameter. The Projected Pupil Plane Pattern (PPPP) offers an alternative solution by projecting a collimated laser beam across the telescope's entire pupil. One significant challenge is dealing with gain-related issues, necessitating the use of two beam profiles obtained simultaneously from two different distances from the telescope pupil. In this work, we explore the integration of a convolutional neural network (CNN) with experimental data emulating PPPP. We investigate how CNNs can significantly simplify the PPPP design by enabling operation with a single beam profile. These results permit the development of the PPPP concept to use a single beam profile without distance-gain degeneracy. In this work, it is shown that a 10% residual error can be achieved for test data randomly chosen over the SNR range of 4 to 12.

## KEYWORDS

Image processing; instrumentation; adaptive optics; machine learning; astronomy

## 1. Introduction

When looking at objects located far away from Earth, optical telescopes with diameters greater than 1 m are typically needed to either obtain images with sufficient angular resolution or to collect sufficient light within an exposure. In the case of ground-based telescopes, the atmosphere introduces aberrations which deform the wavefront, leading to several undesirable effects but principally a random degradation of the point-spread function (PSF) with a systematic drop in angular resolution; equivalently a degradation in the modulation transfer function at medium to high spatial frequencies.<sup>[1]</sup> This is the origin of image blurring and can be overcome by the use of Adaptive Optics (AO), which processes the measurements from a wavefront sensor (WFS) through a wavefront reconstructor and then generates the correction using a deformable mirror (DM) to compensate a non-flat wavefront.<sup>[2]</sup> A traditional AO WFS will use guide stars – natural or artificial – to obtain the latest measurements of wavefront aberrations. Natural guide stars (NGS) are not always located sufficiently close

**CONTACT** Carlos Gonzalez-Gutierrez  [gonzalezgcarlos@uniovi.es](mailto:gonzalezgcarlos@uniovi.es)  Instituto Universitario de Ciencias y Tecnologías Espaciales de Asturias (ICTEA), Oviedo, Spain.

© 2024 The Author(s). Published with license by Taylor & Francis Group, LLC

This is an Open Access article distributed under the terms of the Creative Commons Attribution License (<http://creativecommons.org/licenses/by/4.0/>), which permits unrestricted use, distribution, and reproduction in any medium, provided the original work is properly cited. The terms on which this article has been published allow the posting of the Accepted Manuscript in a repository by the author(s) or with their consent.

### Nomenclature

|        |                               |       |                                  |
|--------|-------------------------------|-------|----------------------------------|
| PPPP   | Projected Pupil Plane Pattern | CWFS  | Curvature WaveFront Sensing      |
| CNN    | Convolutional Neural Network  | SP-P4 | Single-Profile PPPP              |
| SNR    | Signal to Noise Ratio         | DM    | Deformable Mirror                |
| PSF    | Point-Spread Function         | SCAO  | Single-Conjugate AO              |
| AO     | Adaptive Optics               | PreLU | Parametric Rectified Linear Unit |
| WFS    | WaveFront Sensor              | CPU   | Central Processing Unit          |
| NGS    | Natural Guide-Star            | RAM   | Random Access Memory             |
| LGS    | Laser Guide-Star              | VRAM  | Video Random Access Memory       |
| SH-WFS | Shack Hartmann WFS            | GPU   | Graphical Processing Unit        |
| ANN    | Artificial Neural Network     |       |                                  |

to the object of interest with sufficient brightness, and this restriction promoted the development of artificial alternatives; the laser guide star (LGS) which can be deployed at any arbitrary sky position.<sup>[3]</sup> To create a LGS, a laser is projected through the atmosphere to form a compact beacon and the back-scattered light is analyzed with a conventional WFS design, typically a Shack-Hartmann. Using this artificial alternative to NGS is not identical, however, as the volume of atmosphere traversed by the LGS back to the telescope is smaller than from the NGS: this is known as cone-effect or anisoplanatism.<sup>[4]</sup> As an alternative to LGS, in order to solve the anisoplanatism, a technique known as Projected Pupil Plane Pattern (PPPP)<sup>[5]</sup> was proposed, avoiding the need for multiple LGS<sup>[6]</sup> to fully illuminate the volume as well as easing the complexity of both the wavefront reconstructor and the system design: Neichel et al.<sup>[7]</sup> shows how the LGS asterism must change, alongside the reconstructor, to be optimal and this type of system engineering analysis is mandatory for new, multiple-LGS, narrow-field AO.

In contrast, PPPP uses a wide collimated laser, which is projected from the primary telescope mirror and this mimicking of the NGS illumination allows us to compensate for LGS anisoplanatism. The only variable is the height from which the two beam-profiles are recorded. PPPP also changes the nature of the WFS since the signal is developed on the propagation path rather than the reception path. By using linear reconstruction, it has been shown that it is possible to reconstruct the aberrated wave-front above the telescope both in simulation<sup>[8]</sup> and in a laboratory experiment<sup>[9]</sup> while achieving a similar performance to a Shack-Hartmann WFS (SH-WFS) using a NGS. One of the main issues of PPPP is that it relies on the linear reconstructor to obtain the reconstruction of the atmosphere above the telescope and this has high-noise propagation: for a 4 m primary mirror diameter, to obtain similar performance to a SH-WFS observing a bright star, the 1064 nm projected laser's power is ca. 1 kW<sup>[8]</sup> which has obvious difficulties in implementation. More recently, a new reconstruction method based on artificial neural networks (ANN) has been proposed, showing great results for laser powers reduced by at least one order of magnitude.<sup>[10]</sup>

ANNs are an artificial intelligence technique originally inspired by human neurons,<sup>[11]</sup> although its development during the last years has separated from this idea, coining a new term known as Deep Learning<sup>[12]</sup> where several layers of different types of neurons are stacked to improve the learning ability of the system. ANNs have been widely used in AO systems for different tasks<sup>[13]</sup> including an on-sky demonstration of a tomographic reconstructor operating with multiple WFS in the William Herschel telescope in La Palma.<sup>[14]</sup> These results motivated us to investigate using an ANN in the PPPP project in conjunction with the laboratory PPPP demonstrator,<sup>[15]</sup> which can generate realistic images to test the performance of the ANN developed by Yang et al. in a laboratory environment.

The present article is structured as follows. In [Section 2](#), the PPPP method is explained, giving some insights about the PPPP bench development. [Section 3](#) provides details about the CNN used and its training and learning process. After that, in [Section 4](#), the results of the different

experiments are shown along with Section 5, where those results are discussed and analyzed with detail. Finally, in Section 6, conclusions about the experiments are written and future lines of the PPPP technique are exposed.

## 2. PPPP theory and laboratory implementation

The PPPP method was developed from Curvature Wavefront sensing (CWFS),<sup>[16]</sup> which uses images conjugated to two planes which are independently distant from the pupil. These images can be thought of as beam profiles. In the PPPP case, the distances from the pupil to each beam profile are both positive and the profiles are recorded back at the telescope through back-scattering in the free-atmosphere, as in Figure 1. The wavefront sensing method is developed by illuminating through a source of aberrations – typically the atmosphere – and the diffraction causes intensity variations in the beam profiles. Using the transport of intensity equation,<sup>[17]</sup> the following relationship can be developed,

$$k\partial_z I = -\nabla \cdot (I\nabla\phi), \quad (1)$$

where  $k$  is the scalar wave-vector,  $I(x, y; z=0)$  is the intensity recorded at the pupil ( $z=0$ ), and  $\phi(x, y; z=0)$  represents the phase. Implicitly, the phase is determined as co-located with the pupil, hence  $z=0$ . This equation can be approximated as,<sup>[16]</sup>

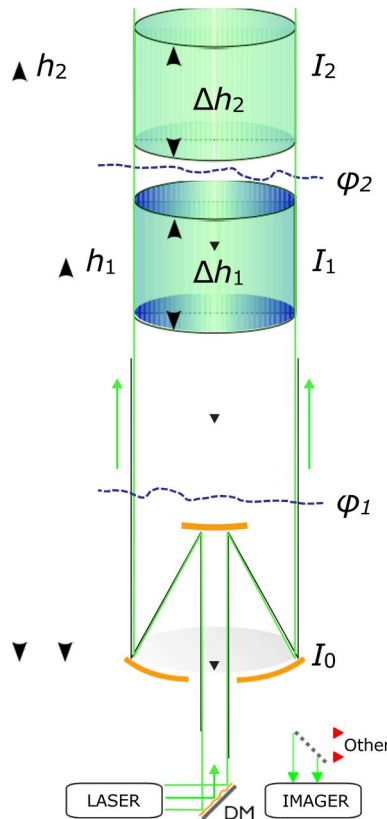


**Figure 1.** Conceptual outline of the PPPP method for wavefront sensing. A collimated laser beam is emitted from a telescope and, as it passes through aberrating layers in the atmosphere,  $\phi_i$ , it diffracts which imparts additional intensity variations at distances  $h_1$  and  $h_2$ . Using time-gating or some similar procedure, the back-scattered intensity from depths  $\Delta h_1$  and  $\Delta h_2$  is received back in the telescope and imaged to produce beam-profiles from the two altitudes. These profile intensities are then combined to produce information on the wavefront derivatives of  $\phi_i$ ,  $d\phi_i/dr$ . The magnitude of  $d\phi_1/dr$  is not dependent on the distance of  $\phi_1$  from the telescope pupil, as is desired, but the magnitude of  $d\phi_2/dr$  is dependent on its distance from both  $h_1$  and  $h_2$ . Single-Profile PPPP (SP-P4) using the beam-profile from  $h_2$  alongside a pre-determined equivalent at the telescope pupil ( $h_1 = 0$ ) would similarly have a magnitude–distance degeneracy for measurements of both  $\phi_1$  and  $\phi_2$ , and the required profile imaging is technologically easier to implement (temporally controlled only by e.g. pulse repetition rate).

$$k \frac{I_2 - I_1}{h_2 - h_1} = -\nabla \cdot (I_0 \nabla \phi), = -\nabla I_0 \cdot \nabla \phi - I_0 \nabla^2 \phi, \quad (2)$$

$$M(I_1, I_2; h_1, h_2; k) \frac{I_2 - I_1}{K h_2 - h_1}$$

where  $M$  is the wavefront derivatives measurement from the detected intensities of the beam profiles,  $I_1(x, y) \equiv I(x, y; h_1)$  and  $I_2(x, y) \equiv I(x, y; h_2)$  as a linear sum of the product of intensity and intensity derivative with wavefront gradient,  $\nabla \phi/k$  and the wavefront second derivative,  $\nabla^2 \phi/k$ , respectively.

## 2.1. PPPP fundamentals

The key factor in Equation (2) is that two beam profiles corresponding to different propagation distances from  $z=0$  can produce a measurement proportional to the wavefront differential along the wavevector. What is less clear is that results from references<sup>[8]</sup> show that the distance of the source of  $\phi$  from the pupil is irrelevant, i.e.  $\phi(x, y; z) \rightarrow \phi(x, y; 0)$  as long as  $z \leq h_1$ . This validates the assumption in Equation (1). For  $h_1 < z < h_2$ , the sensitivity of the measurement to  $\phi(z)$  decreases linearly to zero as  $z \rightarrow h_2$ . This breaks the assumption, but not such that would cause positive feedback if attempting to use it for correction. The overall implication is that only  $\phi$  below both beam-profile distances can be measured accurately: between the profiles, there is an unknown gain term,  $0 \leq 1$ , in the measurement. This situation does not exist for the CWFS, so it is a new phenomenon.

Also, unlike the CWFS method, both terms on the right-hand side of Equation (2) are used simultaneously, which leads to more information per measurement element of the WFS: it is logical to have a detector grid which is compatible with array imaging rather than tied to some polynomial measurement basis, e.g. as shown in reference,<sup>[18]</sup> although this aspect has not been studied.

Finally, to solve for  $\phi$ , the theoretical method of<sup>[19]</sup> from the CWFS literature was used by<sup>[8]</sup> in simulation whereas an interaction matrix approach as with conventional DM-WFS calibration was implemented by Yang et al.<sup>[32]</sup> for operation on the experimental test-bench. Such a use of a pre facto calibrated control approach is standard for experimental work so we do not comment on it further here.

The implementation of PPPP requires two related technologies: a pulsed laser and a detector which can separate in time the back-scattered return from the two distances. The latter is technically difficult, whereas the former is a more standard technology. Therefore, we were motivated to explore if using just one beam profile is possible, i.e.  $h_1 = 0$  which implies we know the outgoing laser beam profile and are only required to measure the beam profile from  $h_2$ . The obvious detriment is that the measurement becomes sensitive to the altitude since  $0 < z < h_2$ : in other words, a degeneracy between the distance to  $\phi$  and the amplitude of  $\phi$  wherein without additional constraints, it is not possible to unambiguously determine an effective gain of  $\phi$ . However, if the aberration distance can be constrained, then single-profile PPPP (SP-P4) would be far simpler to implement since the detector would only be required to be synchronised with the laser pulse emission and no longer with the pulse propagation distance between profiles.

## 2.2. Alternative to overcoming the distance–strength degeneracy

The key issue with using a collimated beam for SP-P4 is that a degeneracy develops between  $h_2 - z$  and  $|\phi|$ ; between the distance from  $\phi$  to  $h_2$  and the amplitude of  $\phi$ . To overcome this, consider instead of one beam profile from a non-zero distance and originating from one illuminating beam (this is SP-P4), one beam profile from the same non-zero distance but now originating from two illuminating, overlapping beams, with these beams having different focal distances, as in Figure 2.

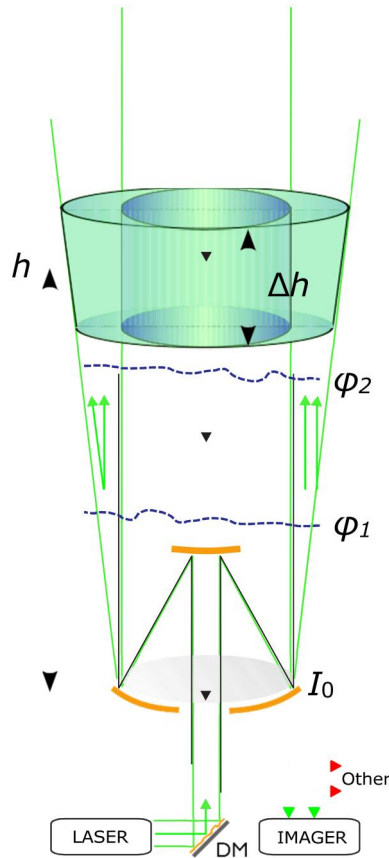


**Figure 2.** Conceptual outline of a modified method for wavefront sensing using one beam-profile and two illuminating beams. Two laser beams are emitted from a telescope, one collimated and one diverging, and as with PPPP they diffract to produce intensity variations in the beams at the distance,  $h$ . The back-scattered intensity from those two beams – but one distance – from a finite volume represented by  $\Delta h$ , is received back in the telescope and imaged to produce a beam-profile from both beams. These combined beam's profile intensities are then used with a non-linear algorithm, such as an ANN, to produce information on the wavefront measurement of  $\phi_i$ 's. Unlike with PPPP, the two use of two beams will break the distance-magnitude degeneracy, which should permit both the correct magnitude of  $\phi_i$ 's to be determined, and also potentially their distance from the telescope.

As with SP-P4 or PPPP (two beam profiles, one illuminating beam), one beam has infinite focus – it is collimated – but now we consider that the other has some divergence. It is known that the diffraction effects – also called scintillation when amalgamated – cause an increase in scintillation with focused beams and, conversely, a reduction with diverging beams.<sup>[20]1</sup>

The outcome is that the distance–strength degeneracy can be broken by sampling the beam profile from a collimated and a diverging/focused beam at the same physical distance from the telescope as in the figure. This might seem to be as complex as PPPP since either switching beams in time or wavelength would be required, but here we propose the advantage of ANNs is that the beams can be superimposed and just one beam profile recorded containing the diffraction effects from both the illuminating beams. Whether the beams are temporally coherent or not is a separate matter to be investigated, but combining the beams on the detector leads to a situation where no known linear reconstructor exists to retrieve  $\phi_i$ 's, and so a machine learning process becomes valuable to investigate this concept. This is particularly pertinent in the non-linear case of the two beams coherently interfering. In the context of this work, by demonstrating PPPP with an ANN in a laboratory, we give confidence for the development of the two-beam single-profile variant that relies on a machine-learning non-linear algorithm, such as an ANN.

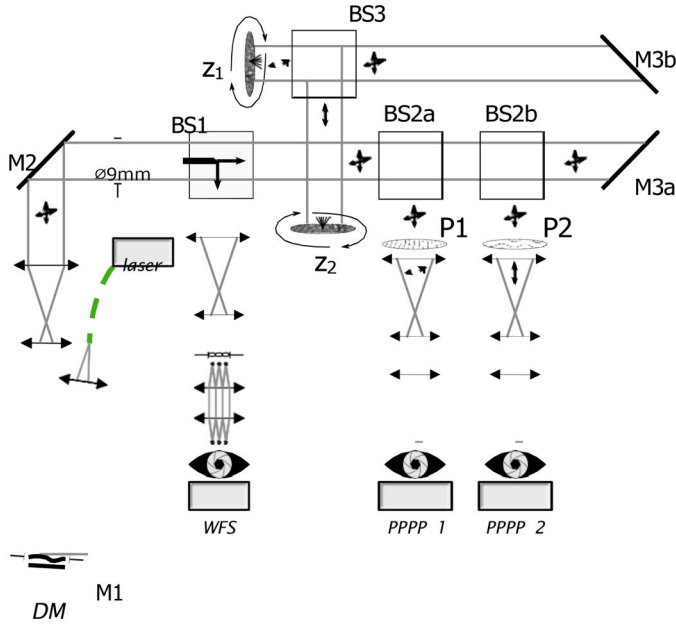


**Figure 3.** Diagram of the layout of the experiment. Principal components are the light source (laser), the deformable mirror (DM, M1), the Shack–Hartmann wavefront sensor arm (WFS), and the two identical PPPP arms (PPPP 1 and 2), which are conjugated to the retro-reflective surfaces  $z_1$  and  $z_2$ . The separation of the scattering from each retro-reflective surface is via polarisation, first separated using BS3 and subsequently by linear polarisers P1 and 2. (Light which is lost and absorbed by beam blockers, preventing erroneous ghosting and stray reflections, is not shown.)

### 2.3. Laboratory implementation

The laboratory experiment for PPPP, [Figure 3](#), was previously used in Yang et al.<sup>[32]</sup> but with modifications, therefore, it is described here for reference. A light source (laser, 635 nm, random polarisation) is collimated and reflected from M1, which is the deformable mirror (DM, DMP40/M-P01 from Thorlabs). The DM is used to inject random aberrations into the path and so represents our source of turbulence: it is not used for correction in this work, and we use both the bimorph actuators which deform the primary mirror surface and the tip/tilt actuators that rotate the mirror surface. The aberrations were chosen to have a white-noise spectrum, which is independent of any assumptions. Following the DM, a pupil image is created where a stop is placed to define the pupil; in this work, 9 mm in diameter. At the first beam-splitter, BS1, 10% of the flux is directed to a Shack-Hartmann WFS with  $7 \times 7$  sub-apertures. The measured centroids, 74 in total, are used in the ANN as the target to train and validate the PPPP estimation. The remainder of the flux is principally diverted via mirrors, M3's, and then a polarising beam-splitter, BS3, to two rotating, retro-reflecting surfaces,  $z_1/2$ , whose linear, orthogonal polarisation state is retained on reflection. The surface is equivalent to 3 M Scotchlite and the rotational motion eliminates laser speckle. The beam-splitters, BS2's, in conjunction with polarisers, P1/2, ensure the back-scatter from each surface is independently imaged by a separate camera. The images from these cameras – the beam-profiles, as it can be seen in [Figure 4](#) – are then processed to form the input into the ANN, together with the WFS centroids as the training outputs, as described in the next section.

## 3. Artificial Neural Networks

One of the main features of ANNs are their ability to learn from a known set of data and apply that knowledge to unseen data with the same characteristics. This process is known as training,

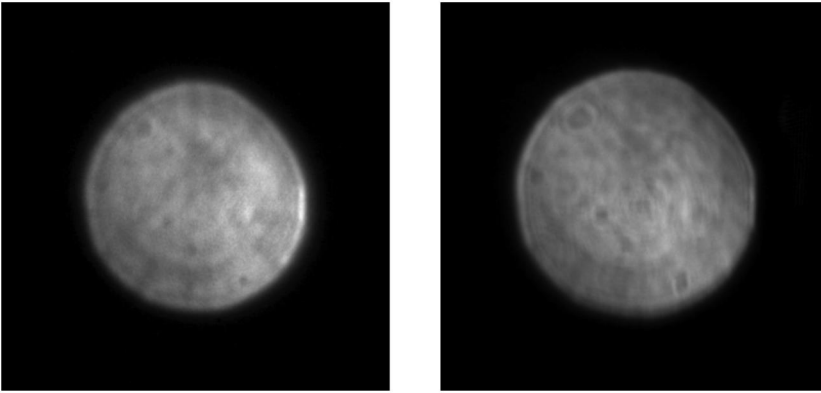


**Figure 4.** Images captured by P1 (left) and P2 (right) show how the laser is affected by the turbulence introduced through the deformable mirror using the procedure explained in Yang, Bharmal, et al. (2019). These images are used as inputs to the neural network, along with the centroids obtained from the Shack-Hartmann as outputs, they provide the necessary information for training

and it is carried out with several pairs from input–output data. By doing this, the ANN acquires the ability to generalize, so it can predict an output when provided an input that has never been used for training. In particular, Convolutional Neural Networks (CNN) are a subtype of ANNs and have shown an excellent performance in recent years for their use in AO, going from the simulation experiment developed by Yang et al. for PPPP, to other approaches like the developed by<sup>[21]</sup> for SCAO configurations or its use by Suárez Gómez et al.<sup>[22]</sup> with a tomographic pupil image WFS.

### 3.1. Convolutional Neural Networks

Convolutional Neural Networks are formed by neurons that learn to self-optimize.<sup>[23]</sup> These networks contain one or several convolutional layers in addition to other type of layers such as pooling, fully connected, or nonlinear.<sup>[24]</sup> Convolutional layers reduce the number of components from the input vector by passing a logistic regression over the whole data.<sup>[25]</sup> CNN are based on the animal visual cortex and are commonly used for processing data that has a grid pattern, such as images.<sup>[26]</sup>

CNNs are based on three different concepts: local receptive fields, shared weights and bias, and pooling. To obtain an output vector with fewer dimensions, the network selects a specific region of the input and connects it to a hidden neuron which learns the field weight and its overall bias. The network's division and the number of hidden layers depend on two different parameters: the kernel size, the size of the region, and the strides, the number of pixels it skips between each receptive field. Each hidden neuron identifies the same feature but in different areas of the image. As a result, between the first hidden layer and the input ones, we find what we call the feature map, defined by the shared bias and gathering all the shared weights. These shared components depict the kernel or filter of the layer. Using shared bias and weights decreases potentially the number of parameters in the network. The last crucial concept when defining the CNN are the pooling layers, which only condense and simplifies the information sent after a convolutional layer.

Using a data set of known inputs and associated outputs, the network trains, learns and adapts its weights trying to optimize its residual error when comparing the output of the neural network with the ideal from the dataset. The correction of the weights leads to the back propagation algorithm<sup>[27]</sup> where the error travels back through the network updating

the values of the weights so it can reduce the obtained error. This operation is repeated until this process has been fully iterated through all the data set and so an “epoch” concludes. Then, the centroids from the WFS can be compared with those obtained by the network in order to reduce the residual error.

### 3.2. Neural network architecture

The CNN used for this application is a combination of different types of layers. After testing several options and connections, it has been concluded that the following architecture is the one that has obtained the best results.

The input consists of pairs of beam profiles, captured by the two PPPP cameras as shown in [Figure 3](#), representing propagation to two different distances from the DM. Different combinations of these images have been used as input, such as the parallel use of the two images and a subtraction between them were tested, along with an experiment that only used the further distance propagated image (from camera PPPP 2). The images have a size of  $300 \times 300$  pixels.

The use of five consecutive convolutional layers reduces the number of parameters trained in the first fully-connected layer of the ANN since it reduces the size of the input image. The number of filters used in these layers increment from one to the other. It begins with eight filters, and it reaches 256. It has been deduced that this increase cannot be very drastic, as it deteriorates the efficiency of the ANN. Also, different kernel or filters sizes and strides or steps have been examined, balancing between profitable computational costs and a minimization of the error measured. Every convolutional layer employs a Parametric Rectified Linear Unit activation function or PreLU.<sup>[28]</sup> The 256 images of  $5 \times 5$  pixels acquired of the sequence of convolutional layers is then flattened into a one-dimension vector of size 6400. This enables the use of two fully connected layers of 128 and 74 neurons consecutively that connect our network with the output layer. A summary of this architecture can be observed in [Table 1](#). The 74 neurons in the last layer relate to the 74 centroids from the WFS in the experiment.

This network has been created using *TensorFlow* software.<sup>[29]</sup> The finest results have been obtained with a learning rate equal to 0.000025, with a momentum of 0.5 and a batch size of 64. Also, a normalization factor has been used in order to enhance the performance of the network. One important tweak used to enhance the performance of the CNN is to create a custom error

**Table 1.** Final network. Number of output filters, size of the filters and strides are indicated in each convolutional layer.

|                                 |
|---------------------------------|
| Input images ( $64 \times 64$ ) |
| Conv2D (8, $3 \times 3$ , 2)    |
| ELU                             |
| Conv2D (32, $3 \times 3$ , 1)   |
| ELU                             |
| Conv2D (64, $3 \times 3$ , 1)   |
| ELU                             |
| Conv2D (128, $5 \times 5$ , 3)  |
| ELU                             |
| Conv2D (256, $5 \times 5$ , 4)  |
| ELU                             |
| Flatten                         |
| Dense (128)                     |
| ELU                             |
| Dense (256)                     |
| ELU                             |
| Flatten                         |
| Output vector (74)              |

function which minimizes the residual wavefront error (WFE) after converting the centroids to a re-constructed phase. To train the neural network, the 74 neurons (both from the CNN and the WFS measurements) at the output are transformed into a wavefront and then both are compared to obtain the residual WFE, which is the value backpropagated and used to update the weights of the CNN.

### 3.3. Training and test data

Training and test sets have been created in an optical bench as the one described in Figure 3. To generate this data, five different values of SNR in the measured WFS slopes (4.2, 6.7, 8.3, 10.0, 12.5) were used to train the network for variable atmospheric turbulence strength. Noise was added after measurements to ensure control of the SNR per dataset. For each SNR value, 40,000 random input phases resulted in the same number of image pairs (beam profiles), totaling 200,000 image pairs for the five strengths.

This complete set was split as follows to test the performance of the ANN:

- Out of the 200,000 image pairs, 20,000 randomly chosen pairs were saved for testing. These pairs are kept apart and used for the different experiments, allowing cross-comparison. These data set will be known as the 'Random' test set.
- Removing 20,000 image pairs generated for a specific SNR (out of 40,000) for testing. These data are known as 'SNR<sub>x</sub>' test set.

In either case, the remaining 180,000 image pairs were used for training, utilising 5% of these for validation during the training process. It is important to remark that the test sets are never used as part of the training data.

### 3.4. Real time performance

Although the main goal of this article is not to probe how PPPP can be implemented in a real system, it is quite interesting to analyze how fast an actual output can be obtained from a single image. To perform that measurement *PyTorch*<sup>[30]</sup> has been used as inference tool along with a server equipped with a Intel(R) Xeon(R) W-3235 CPU @ 3.30 GHz, with 512 Gb of RAM and one Nvidia RTX 2080 GPU. All the weights of neural network were previously loaded in the graphics card VRAM before providing the input image and the experiment were conducted feeding the NN with 1,000 images one at a time. It was possible to obtain the outputs in less than two seconds, which give an average of 2 milliseconds per output. This result is sufficient for real-time systems that operate up to 500 Hz such as MOR- FEO/MAORY<sup>[31]</sup> encouraging the feasibility of the solution, having still margin of improvement for the implementation of the system in a real telescope, since it will be possible to create an *ad hoc* code for the neural network instead of using *PyTorch*, along with the acquisition of newer and more powerful and updated GPUs.

## 4. Experiment and results

The work of Yang et al.<sup>[1]</sup> used experimental data with a linear algorithm, which mandated using both beam profiles in an image pair, but using an ANN, it is possible to design a wider number of data analysis experiments including using one input image rather than two. Here we used two additional inputs to the ANN: subtraction of the two beam profiles in an image pair (difference), or using the beam profile corresponding to further propagation ( $z_2$ , from camera PPPP 2). Of the

two beam profiles, we chose the one which has a higher SNR and this is equivalent to SP-P4 because the implicit  $I_0$  is just a constant value in this configuration.

These two experiments (difference and single) allow us to provide new results when analyzing its performance in different case scenarios as described in the previous section. We should add that because the SH WFS is not calibrated, the results are at the plate scale of the WFS which is unknown in angular units. Of interest in this work is the relative precision and accuracy of the ANN estimation, so physical units are not necessary, as the WFS SNR is reported here. In this scenario, the residual error refers to the residual wavefront error, which is obtained by subtracting the centroids predicted by the neural network from those provided by the SH-WFS and converted into a wavefront.

#### 4.1. Two images, both beam profiles

In this experiment, both beam profiles in each image pair are used as the CNN input. Results can be seen in Table 2.

When using two images as it was done in the original experiments, the performance of the ANN results in no correction which is consistent with the ANN resolving no output except for the case of the random test set.

#### 4.2. Subtracted image, the difference

For the second experiment, the difference in each image pair is used as the input. Results can be seen in Table 3.

The behaviour of the ANN in this scenario is quite erratic. It is noted that the images are normalised in total power before subtraction: this corresponds to the numerator of Equation (2), which implies a proportionality to the wavefront derivatives. At higher SNR, some correct estimation is made, but there is no clear relationship with noise, and for the lowest SNR, the ANN is able to retrieve a partial estimate, although it is not complete.

#### 4.3. One image, a single beam profile

In this experiment, only one of the two images in the pair is used, and this is equivalent to SP-P4. Results can be seen in Table 4.

The results of the ANN with this input configuration have the best performance of all three. In the random test set case, the correction approaches the expectation of noise error, 0.05 based on discrete centroid curl.<sup>[32]</sup> The other interesting result is that residual is not correlated with SNR, implying noise does not affect the ANN estimation. This implies the ANN will be robust against noise and with the ability to be trained to accommodate variable input amplitude, shown by the random test-set result.

**Table 2.** Two images as input results.

| Test set | Residual error | Non corrected error | WFE percentage |
|----------|----------------|---------------------|----------------|
| Random   | 0.156          | 0.491               | 31.77          |
| SNR 4.3  | 0.191          | 0.214               | 88.94          |
| SNR 6.7  | 0.310          | 0.320               | 97.08          |
| SNR 8.3  | 0.573          | 0.576               | 99.51          |
| SNR 10.0 | 0.575          | 0.580               | 99.31          |
| SNR 12.5 | 0.742          | 0.746               | 99.41          |

**Table 3.**  $I_2-I_1$  as input results.

| Test set | Residual error | Non corrected error | WFE percentage |
|----------|----------------|---------------------|----------------|
| Random   | 0.120          | 0.491               | 24.37          |
| SNR 4.3  | 0.151          | 0.214               | 70.57          |
| SNR 6.7  | 0.231          | 0.320               | 72.45          |
| SNR 8.3  | 0.752          | 0.576               | 130.61         |
| SNR 10.0 | 0.281          | 0.580               | 48.40          |
| SNR 12.5 | 0.264          | 0.746               | 35.38          |

**Table 4.**  $I_2$  as input results.

| Test set | Residual error | Non corrected error | WFE percentage |
|----------|----------------|---------------------|----------------|
| Random   | 0.052          | 0.491               | 10.70          |
| SNR 4.3  | 0.156          | 0.214               | 72.86          |
| SNR 6.7  | 0.201          | 0.320               | 62.77          |
| SNR 8.3  | 0.265          | 0.576               | 46.01          |
| SNR 10.0 | 0.167          | 0.580               | 28.76          |
| SNR 12.5 | 0.119          | 0.746               | 15.90          |

## 5. Discussion

In the previous section, results from the neural network have been shown for the three experiments, and only the use of the single beam profile from the image pairs produces a useful estimation. Using both beam profiles as inputs seems to complicate the learning process of the CNN and with real data the ability to generalise is almost non-existent despite what was shown with simulated data Yang et al.<sup>[15]</sup> With these results, we conclude the ANN as described is unable to operate with two separate images in a real-world implementation.

In the case of the beam profile differences ( $I_2-I_1$ ), it is possible to observe an improvement when compared with the previous experiment. When changing the value of the SNR in the different datasets, the ANN starts to show acceptable performance, especially when dealing with high turbulent atmospheres and in the case of random testing, which shows the best performance of all. It is interesting to see how the fact of using only a single image that has been created from the subtraction of the two actual images provides enough information for the neural network to partially correct the turbulence, especially in cases where the signal of that turbulence is high.

The best results occur from the third experiment, single beam profile ( $I_2$ ) as input for the ANN. With the random test set, the performance of the system is close to the limit of the WFS noise (which limits the fundamental performance). This shows the potential of the neural network, since it indicates having a sufficiently large and diverse training set allows sufficiently good performance in comparison with a linear measurement from a conventional wavefront sensor. Unusually this occurs when only using a single beam profile. Also in this scenario, the CNN estimation is consistent with the input SNR although there is a baseline error which cannot be removed with the training dataset obtained. (It should be noted that due to experimental and logistical limitations, the dataset size of 200,000 image pairs was the technical limit.) The consistency in estimation with the SNR is consistent with other AO studies such as reference.<sup>[14]</sup> Our results also agree with the experiments done in Yang et al.,<sup>[1]</sup> which show that the ANN is able to work with a single image and this mode of operation is confirmed in this article.

Although the original PPPP concept required two images (beam profiles) as inputs for the reconstruction, the ANN is able to work with a single beam profile, and it obtaining high performance is encouraging. As previously explained, the technical complexity for obtaining two beam profiles can then be avoided, what gives confidence that the Wavefronts Obtained from Measurements from Beam-profiles through Atmospheric Turbulence (WOMBAT) concept, of using two illuminating beams and recording one beam profile to overcome the distance-strength

degeneracy implicit in SP-P4, can be implemented with the CNN architecture described, although uncertainty remains as to whether it can truly eliminate the distance–gain degeneracy.

## 6. Conclusions and future lines

In this article, we have shown the potential of applying an ANN to the PPPP technique when using data generated from an experimental test-bed in the laboratory.

This combination (ANN and PPPP) has already been tested in simulation, and it was a natural step to analyze its behaviour when using real data. Using two beam profiles, as in the reconstructor of the original proposal, results in poor reconstruction estimation. However, using a single image, SP-P4 is a potential solution that overcomes the reconstruction error. An ANN is, therefore, a useful solution with real-world data to estimate the wavefront but under certain conditions that introduce measurement limitations with PPPP. In this work, we have proposed a related concept, WOMBAT, which overcomes the distance–strength degeneracy, and only produces one beam profile. Our main result, which we have demonstrated with laboratory data, is that the measurement analysis concept is feasible here. The additional benefit of the ANN over the linear reconstructor previously demonstrated is the improvement in operation at low SNR. In future work, we plan to further test the WOMBAT concept and understand the SNR limitations to place a better bound on potential minimum laser power required.

## Note

1. Alternately this can be described by the Huygens-Fresnel principle and the reduction in size of the first 1/2-period zone.<sup>[33]</sup>

## Acknowledgements

N.A. Bharmal, T.J. Morris, and L.W. Fitzpatrick acknowledge UKRI Science and Technology Funding Council grants ST/T000244/1 and ST/X001075/1. Data from the PPPP cameras (1 and 2), WFS, and supporting material are available online from the Durham University research data repository, <http://doi.org/10.15128/r2np193923h>. N.A. Bharmal thanks the Department of Physics, Durham University for making the laboratory experiment safely accessible in- person during the COVID-19 restrictions in 2020, during which time the experiment was operated.

## Disclosure statement

The authors declare no conflicts of interest.

## Funding

C. González-Gutiérrez, J. Rodríguez-Muro, A. Buendía-Roca, and F.J. de Cos Juez would like to acknowledge the projects MCIU-22-PID2021-127331NB-I00 funded by AGENCIA ESTATAL DE INVESTIGACION (M°. ECON. IND.) and SV-PA-21-AYUD/2021/51301 funded by FUNDACION PARA LA INVESTIGACION CIEN-TIFICA Y TECNICA FICYT. N.A. Bharmal, T.J. Morris, and L.W. Fitzpatrick acknowledge UKRI Science and Technology Funding Council grants ST/T000244/1 and ST/X001075/1.

## References

- [1] Hardy, J. W. *Adaptive Optics for Astronomical Telescopes on Demand*. (Vol. 16). Oxford University Press, 1998.
- [2] Rigaut, F. Astronomical adaptive optics. *Publ. ASP.* **2015**, 127, 1197.

- [3] Fugate, R. Q.; Fried, D. L.; Ameer, G. A.; Boeke, B. R.; Browne, S. L.; Roberts, P. H.; Ruane, R. E.; Tyler, G. A.; Wopat, L. M. Measurement of atmospheric wavefront distortion using scattered light from a laser guide-star. *Nature* **1991**, 353, 144–146. DOI: [10.1038/353144a0](https://doi.org/10.1038/353144a0).
- [4] Fried, D. L.; Belsher, J. F. Analysis of fundamental limits to artificial – Guide-Star adaptive-optics-system performance for astronomical imaging. *J. Opt. Soc. Am. A.* **1994**, 11, 277–287. DOI: [10.1364/JOSAA.11.000277](https://doi.org/10.1364/JOSAA.11.000277).
- [5] Buscher, D. F.; Love, G. D.; Myers, R. M. Laser beacon wave-front sensing without focal anisoplanatism. *Opt. Lett.* **2002**, 27, 149–151. <https://opg.optica.org/abstract.cfm?URI=ol-27-3-149>. DOI: [10.1364/ol.27.000149](https://doi.org/10.1364/ol.27.000149).
- [6] Foy, R.; Labeyrie, A. Feasibility of adaptive telescope with laser probe. *A & A* **1985**, 152, L29–L31.
- [7] Neichel, B.; Fusco, T.; Sauvage, J.-F.; Correia, C.; Dohlen, K.; El-Hadi, K.; Blanco, L.; Schwartz, N.; Clarke, F.; Thatte, N. A.; Tecza, M.; Paufigue, J.; Vernet, J.; Le Louarn, M.; Hammersley, P.; Gach, J.-L.; Pascal, S.; Vola, P.; Petit, C.; Conan, J.-M.; Carlotti, A.; Véronaud, C.; Schnetler, H.; Bryson, I.; Morris, T.; Myers, R.; Hugot, E.; Gallie, A. M.; David M. Henry. The Adaptive optics modes for Harmoni: From classical to laser assisted tomographic AO. *Adapt. Optic. Syst. V.* 2016, 9909, 92–106. DOI: [10.1117/12.2231681](https://doi.org/10.1117/12.2231681).
- [8] Yang, H.; Bharmal, N. A.; Myers, R. M. Projected pupil plane pattern: An alternative LGS wavefront sensing technique. *Month. Notices Royal Astron. Soc.* **2018**, 477, 4443–4453. Retrieved from <https://academic.oup.com/mnras/article/477/4/4443/4969700>. DOI: [10.1093/mnras/sty926](https://doi.org/10.1093/mnras/sty926).
- [9] Yang, H.; Bharmal, N. A.; Myers, R. M.; Basden, A.; Buscher, D.; De Cos Juez, F. J.; ... Younger, E. LGS alternative wave-front sensing: Projected Pupil Plane Pattern (PPPP). *Adapt. Optic. Syst. VI.* 2018, 26. Retrieved from [10.1117/12.2311991.full](https://doi.org/10.1117/12.2311991.full).
- [10] Yang, H.; Gonzalez-Gutierrez, C.; Bharmal, N. A.; de Cos Juez, F. J. Projected pupil plane pattern (PPPP) with artificial neural networks. *Month. Notices Royal Astron. Soc.* **2019**, 487, 1480–1487. Retrieved from <https://academic.oup.com/mnras/advance-article/doi/10.1093/mnras/stz1362/5497305>. <https://academic.oup.com/mnras/article-abstract/487/1/1480/5497305>. DOI: [10.1093/mnras/stz1362](https://doi.org/10.1093/mnras/stz1362).
- [11] Rosenblatt, F. The perceptron: A probabilistic model for information storage and organization in the brain. *Psychol. Rev.* **1958**, 65, 386–408. DOI: [10.1037/h0042519](https://doi.org/10.1037/h0042519).
- [12] LeCun, Y.; Bengio, Y.; Hinton, G. Deep learning. *Nature* **2015**, 521, 436–444. Retrieved from <http://www.nature.com/doi/10.1038/nature14539>. DOI: [10.1038/nature14539](https://doi.org/10.1038/nature14539).
- [13] Suárez Gómez, S. L.; González-Gutiérrez, C.; Alonso, E. D.; Santos, J. D.; Rodríguez, M. L. S.; Morris, T.; Osborn, J.; Basden, A.; Bonavera, L.; González, J. G.-N. Experience with artificial neural networks applied in multi-object adaptive optics. *PASP.*, **2019**, 131, 108012. Retrieved from DOI: [10.1088/1538-3873/131/1/108012](https://doi.org/10.1088/1538-3873/131/1/108012).
- [14] Osborn, J.; Guzman, D.; de Cos Juez, F. J.; Basden, A. G.; Morris, T. J.; Gendron, E.; Butterley, T.; Myers, R. M.; Guesalaga, A.; Sanchez Lasheras, F.; et al. Open-loop tomography with artificial neural networks on CANARY: On-sky results. *MNRAS.* **2014**, 441, 2508–2514. DOI: [10.1093/mnras/stu758](https://doi.org/10.1093/mnras/stu758).
- [15] Yang, H.; Bharmal, N.; Myers, R.; Younger, E. Laboratory demonstration of an alternative laser guide stars wavefront sensing technique—Projected pupil plane pattern. *J. Astron. Telesc. Instrum. Syst.* **2019**, 5, 1–10. Retrieved from DOI: [10.1117/1.JATIS.5.2.029002](https://doi.org/10.1117/1.JATIS.5.2.029002).
- [16] Roddier, F. Wavefront sensing and the irradiance transport equation. *Appl. Opt.* **1990**, 29, 1402–1403. DOI: [10.1364/AO.29.001402](https://doi.org/10.1364/AO.29.001402).
- [17] Teague, M. R. Deterministic phase retrieval: A green’s function solution. *J. Opt. Soc. Am.* **1983**, 73, 1434–1441. DOI: [10.1364/JOSA.73.001434](https://doi.org/10.1364/JOSA.73.001434).
- [18] Takami, H.; Takato, N.; Hayano, Y.; Iye, M.; Oya, S.; Kamata, Y.; Kanzawa, T.; Minowa, Y.; Otsubo, M.; Nakashima, K.; et al. Performance of Subaru Cassegrain adaptive optics system. *Publ. Astronom. Soc. Japan.* **2004**, 56, 225–234. DOI: [10.1093/pasj/56.1.225](https://doi.org/10.1093/pasj/56.1.225).
- [19] Gureyev, T. E.; Nugent, K. A. Phase retrieval with the transport-of-intensity equation. ii. Orthogonal series solution for Nonuniform illumination. *J. Opt. Soc. Am. A.* **1996**, 13, 1670–1682. DOI: [10.1364/JOSAA.13.001670](https://doi.org/10.1364/JOSAA.13.001670).
- [20] Andrews, L. C.; Ronald, L. P. 2005. *Laser beam propagation through random media*. 2nd ed. Society of Photo-Optical Instrumentation Engineers. Retrieved from DOI: [10.1117/3.626196.fm](https://doi.org/10.1117/3.626196.fm).
- [21] Riesgo, F. G.; Gómez, S. L. S.; Rodríguez, J. D. S.; Gutiérrez, C. G.; Hernando, Y. M.; Martínez, L. M. M.; Ramos, A. A.; Vera, M. C.; Cagigal, M. N.; Juez, F. J. D. C. Comparative study of Shack–Hartmann configurations for atmospheric turbulence reconstructions in solar adaptive optics. *Opt. Laser Eng.* **2022**, 158, 107157. Retrieved from <https://www.sciencedirect.com/science/article/pii/S0143816622002093>. DOI: [10.1016/j.optlaseng.2022.107157](https://doi.org/10.1016/j.optlaseng.2022.107157).
- [22] Suárez Gómez, S. L.; González-Gutiérrez, C.; Díaz Suárez, J.; Fernández Valdivia, J. J.; Rodríguez Ramos, J. M.; Rodríguez Ramos, L. F. S.; Rodríguez, J. D. Compensating atmospheric turbulence with CNNs for

- defocused pupil image wavefront sensors. *Logic J. IGPL*. **2020**, 29, 180–192. Retrieved from DOI: [10.1093/jigpal/jzaa045](https://doi.org/10.1093/jigpal/jzaa045).
- [23] O’Shea, K.; Nash, R. *An introduction to convolutional neural networks* (Tech. Rep.). 2015. Retrieved from <http://arxiv.org/abs/1511.08458>.
- [24] Albawi, S.; Bayat, O.; Al-Azawi, S.; Ucan, O. N. Social touch gesture recognition using convolutional neural network. *Comput. Intell. Neurosci.* **2018**, 2018, 6973103–6973110. DOI: [10.1155/2018/6973103](https://doi.org/10.1155/2018/6973103).
- [25] Skansi, S. 2018. *Introduction to deep learning*. Springer International Publishing. Retrieved from [10.1007/978-3-319-73004-2](https://doi.org/10.1007/978-3-319-73004-2).
- [26] Yamashita, R.; Nishio, M.; Do, R. K. G.; Togashi, K. Convolutional neural networks: An overview and application in radiology. *Insights Imag.* **2018**, 9, 611–629. DOI: [10.1007/s13244-018-0639-9](https://doi.org/10.1007/s13244-018-0639-9).
- [27] Rumelhart, D. E.; Hinton, G. E.; Williams, R. J. *Learning internal representations by error propagation*. (Tech. Rep.). California Univ San Diego La Jolla Inst for Cognitive Science, 1985.
- [28] He, K.; Zhang, X.; Ren, S.; Sun, J. *Delving deep into rectifiers: Surpassing human-level performance on image-net classification* (Tech. Rep.). 2015. Retrieved from <http://arxiv.org/abs/1502.01852>.
- [29] Abadi, M.; Agarwal, A.; Barham, P.; Brevdo, E.; Chen, Z.; Citro, C.; Corrado, G. S.; Davis A.; Dean J.; Devin M.; Ghemawat S.; Goodfellow I.; Harp A.; Irving G.; Isard, M.; Jia, Y.; Jozefowicz, R.; Kaiser, L.; Kudlur, M.; Levenberg, J.; Mane, D.; Monga, R.; Moore, S.; Murray, D.; Olah, C.; Schuster, M.; Shlens, J.; Steiner, B.; Sutskever, I.; Talwar, K.; Tucker, P.; Vanhoucke, V.; Vasudevan, V.; Viegas, F.; Vinyals, O.; Warden, P.; Wattenberg, M.; Wicke, M.; Yu, Y.; Zheng, X. *TensorFlow: Large-scale machine learning on heterogeneous systems*. 2016. Retrieved from <https://www.tensorflow.org/> (Software available from [tensorflow.org](https://www.tensorflow.org/)).
- [30] Paszke, A.; Gross, S.; Massa, F.; Lerer, A.; Bradbury, J.; Chanan, G.; Killeen, T.; Lin, Z.; Gimeshein, N.; Antiga, L.; Desmaison, A.; Kopf, A.; Yang, E.; DeVito, Z.; Raison, M.; Tejani, A.; Chilamkurthy, S.; Steiner, B.; Fang, L.; Bai, J.; Chintala, S. Pytorch: An imperative style, high-performance deep learning library. *Adv. Neural Inf. Proc. Syst.* 2019, 32, 8024–8035. Curran Associates, Inc. Retrieved from <http://papers.neurips.cc/paper/9015-pytorch-an-imperative-style-high-performance-deep-learning-library.pdf>.
- [31] Hippler, S. Adaptive optics for extremely large telescopes. *J. Astronom. Inst.* **2019**, 08, 1950001. Retrieved from DOI: [10.1142/S2251171719500016](https://doi.org/10.1142/S2251171719500016).
- [32] Bharmal, N. A.; Reeves, A. P. Estimating stochastic noise using in situ measurements from a linear wavefront slope sensor. *Opt. Lett.* **2016**, 41, 428–431. DOI: [10.1364/OL.41.000428](https://doi.org/10.1364/OL.41.000428).